Supporting Information Available

SI-1: Impact of the volume fraction space discretization on the accuracy of phase diagrams

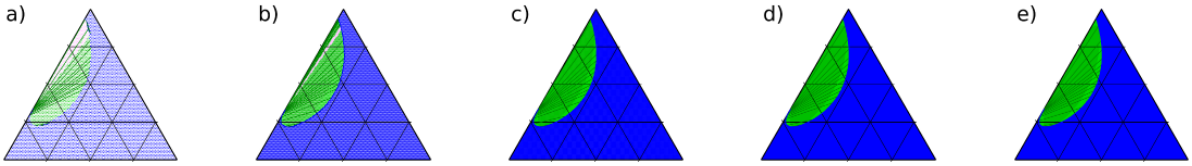

Figure 9: Phase diagram calculated with a discretization of a) 100, b) 200, c) 300, d) 400 and e) 500 grid points in each direction of the volume fraction space.

The discretization of volume fraction space significantly affects both computational time and the accuracy of phase diagrams. A balance must be struck between a coarse discretization that reduces computation time and a finer discretization that improves calculation accuracy. Based on an initial screening of representative phase diagrams, an optimal compromise is achieved with a discretization of 300 grid points along each volume fraction direction. Below this threshold, the likelihood of numerical artifacts increases, as shown in Figure 9. Additionally, using 300 grid points per direction for the phase diagram in Figure 9 reduced computational time by a factor of three compared to a discretization of 500 grid points per direction. Notably, with this choice, numerical artifacts were observed in less than 0.5% of the 81,000 generated phase diagrams.

SI-2: Additional results for the octant-based existence rules

The reported existence rules are based on the number of immiscible pairs of components. For the design space considered in this work, three octants match this rule when one and two

pairs of interaction parameters are above a critical value. In the main paper, only one octant is depicted. This part of SI provides all three octants for each material system considered.

Figure 10 depicts the results for all octants with one interaction parameter above the critical value. Note the general trends for all three material systems, with the three-phase equilibrium region appearing when one interaction parameter is above the critical value ($\bar{\chi} > 1$), while two others are slightly below the critical values ($\bar{\chi}$ slightly below 1). In some cases (Figure 10 - middle row) of the presented results, type [131] is reported for a very narrow range of interaction parameters and only for SM-S-S system. This means that type [131] is less likely when the two materials with the largest molar sizes make up the immiscible pair. Beyond this, type [131] is less typical type for systems with high molar size (P-SM-S) across three octants, with type [110] dominating the parameter space.

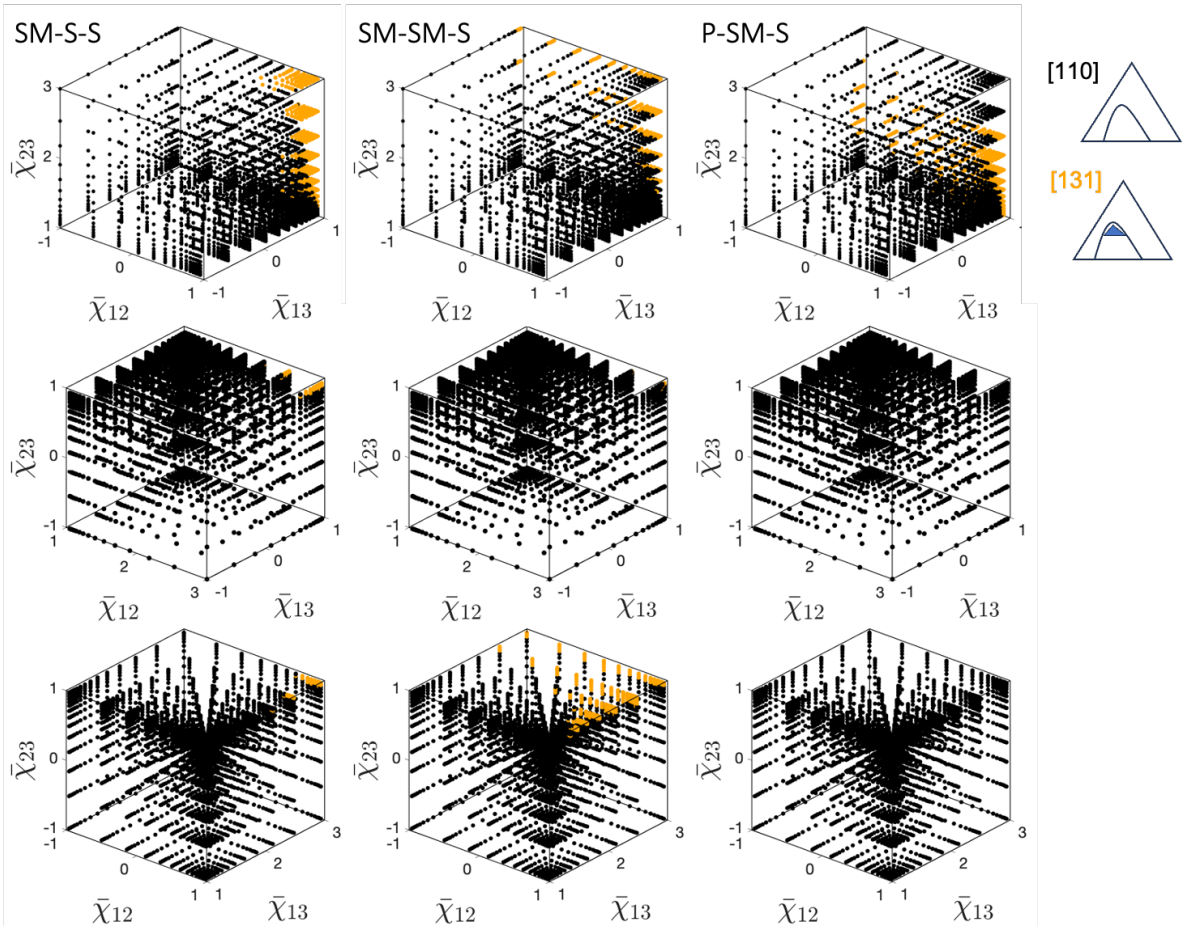

Figure 10: The distribution of the phase diagram types for all octants with one χ_{ij} above χ_{ij}^c): (top) χ_{23} is above the critical value, (middle) χ_{12} is above the critical value and (bottom) χ_{13} is above the critical value.

Similarly, Figure 11 depicts the results for all three octants with two interaction parameters above the critical values χ_{ij} above χ_{ij}^c). The general trends are maintained across the three material systems studied here. Phase diagrams of type [120] with two miscibility gaps are more common when the interaction parameter of the miscible materials pair is only slightly below the critical value. Note the blue points located at the corresponding corners of the octants across all nine panels. Phase diagrams of type [231] are reported in two corners of the presented octants: the three-phase region emerges when one of the interaction parameters above the critical value becomes very large. The central panel of Figure 11 showcases this situation. The deep blue points are located in two corners of the octant, depending on

the origin of the three-phase regions. When the value of $\bar{\chi_{23}}$ is high, the three-phase region links this interaction parameter, while when $\bar{\chi_{13}}$ is high, the three-phase region links to this interaction parameter.

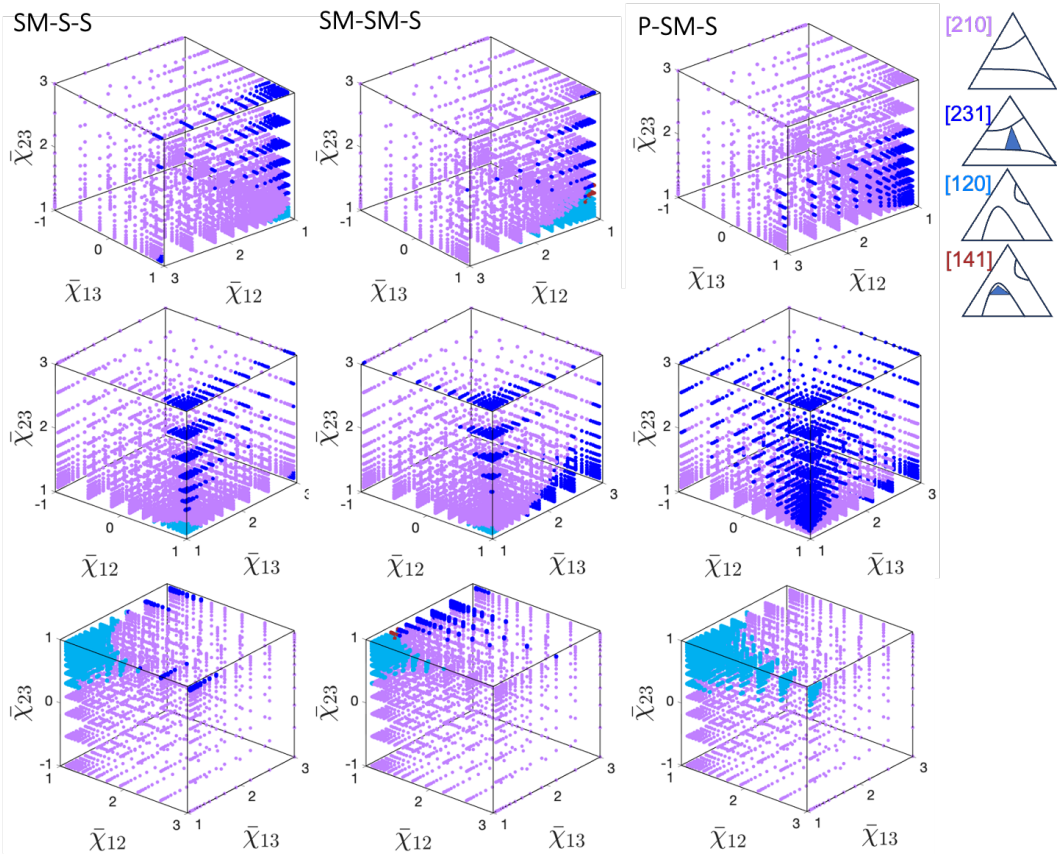

Figure 11: The distribution of the phase diagram types for all octants with two χ_{ij} above χ_{ij}^{c}).

SI-3: Distribution of the phase diagram types at the selected planes for the design space

Figure 12 shows phase diagrams on a plane of the parameter space, corresponding to a fixed value of χ_{12} slightly below the critical value ($\chi_{12} = 0.12408 < \chi_{12}^{c}$) and a selected range for the two remaining interaction parameters. One of the interaction parameters is below its critical value ($\chi_{13} < \chi_{13}^{c}$) while the other is above the critical value ($\chi_{23} > \chi_{23}^{c}$). As χ_{13}

approaches its critical value and χ_{23} is slightly above the critical value (right bottom corner of the figure), the two-phase region is significantly smaller than when χ_{13} is significantly lower (left bottom corner of the figure). This is a typical counter-intuitive situation where increasing the miscibility of one material pair decreases the miscibility of the ternary blend. We attribute this behavior to the underlying mechanism of phase separation, similar to one reported by[4] for the closed-loop isolate miscibility gap. When χ_{13} is significantly lower than the critical value, the phase separation is dominated by the preferential attraction of components 1 and 3 over the other (2 and 3). As χ_{13} increases and approaches the critical value, the three interactions become stronger, resulting in small miscibility gaps. However, this requires additional analytical analysis that we defer to a separate publication.

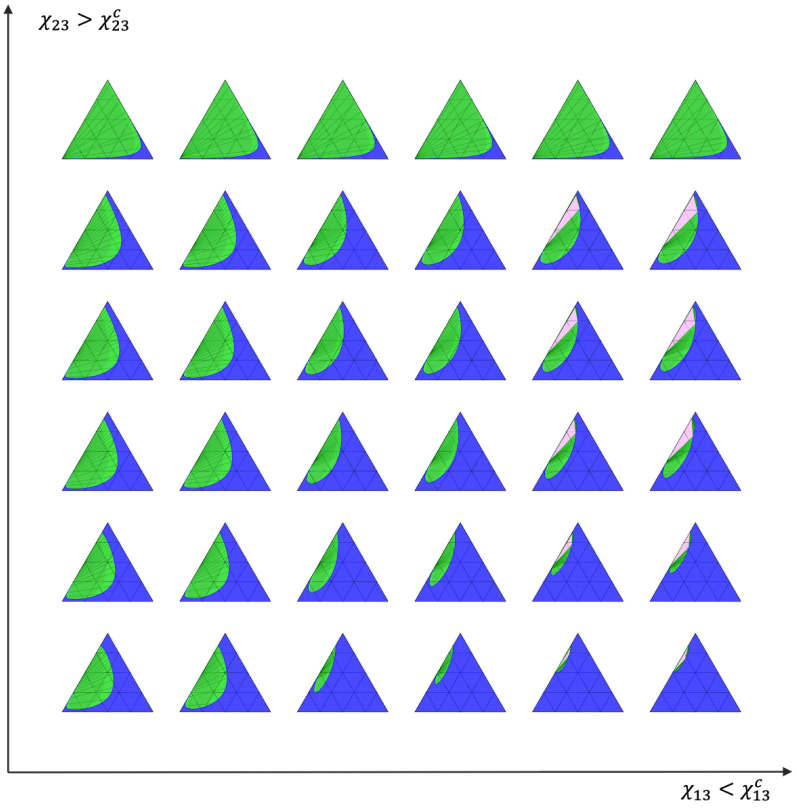

Figure 12: The distribution of the phase diagram types of P-SM-S at the selected plane $\chi_{12} = 0.12408$ ($< \chi_{12}^c$), when one χ_{ij} above χ_{ij}^c). The phase diagrams included in the figure correspond to the following: $\chi_{13} = \{0.052495, 0.17143, 0.46028, 0.48475, 0.5291, 0.53763\}$ $\chi_{23} = \{1.0996, 1.1359, 1.1974, 1.2427, 1.3017, 3.1416\}$.

Similarly, Figure 13 showcases the distribution of phase diagrams when two interaction

parameters are above the critical values. The phase diagrams are selected for a fixed value of χ_{13} slightly below the critical value ($\chi_{13} = 0.53763 < \chi_{13}^c$).The two other interaction parameters vary above the critical value (as noted in the figure). Note the non-trivial distribution of phase diagram types. The type [141] can be found only when three interaction parameters are close to their critical values (left bottom corner). As χ_{23} increases, the two miscibility gaps merge (type [231]) and become larger as expected. Still, then the three-phase regions disappear, as the tie-lines for two two-phase regions align with each other and merge into the two-phase region (see the first column of the figure). This trend is consistent across all the columns in this figure. However, the dominance of the three-phase region depends non-linearly on the relative values of the interaction parameters - as depicted in Figure 10.

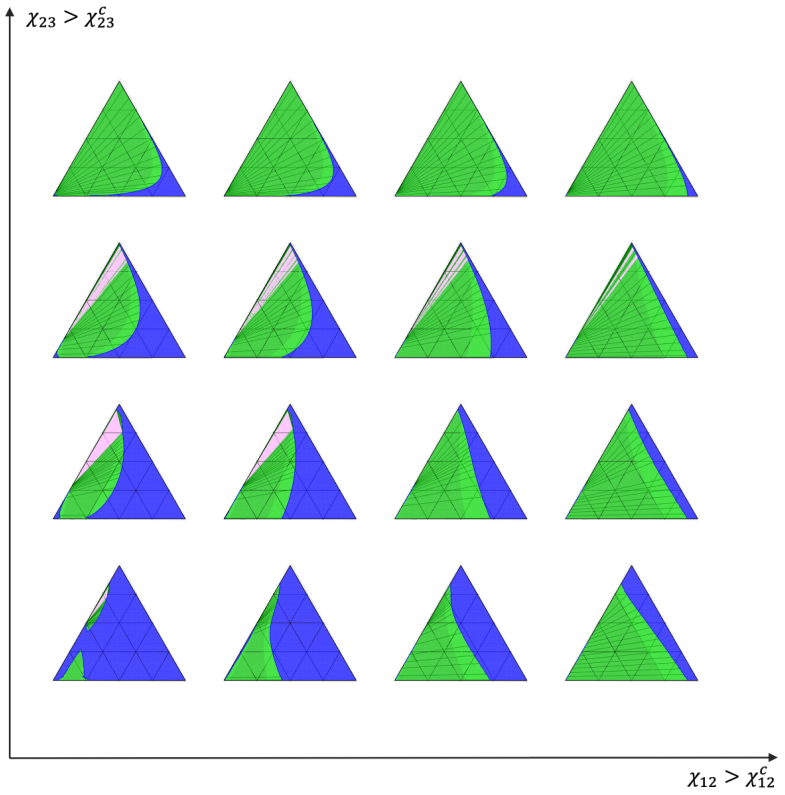

Figure 13: The distribution of the phase diagram types of P-SM-S at the selected plane $\chi_{13} = 0.53763$, when two χ_{ij} above χ_{ij}^c). The phase diagrams included in the figure correspond to the following: $\chi_{12} = \{0.13714, 0.155, 0.22166, 0.39184\}$, $\chi_{23} = \{1.0996, 1.3017, 1.6081, 2.6565\}$.

SI-4: Features of phase diagrams

Figure 7 depicts the definition of the miscibility depth along three composition directions for types [110] and [210]. There are three panels for each type of phase diagram, each panel corresponding to the permutations of the interaction parameters.

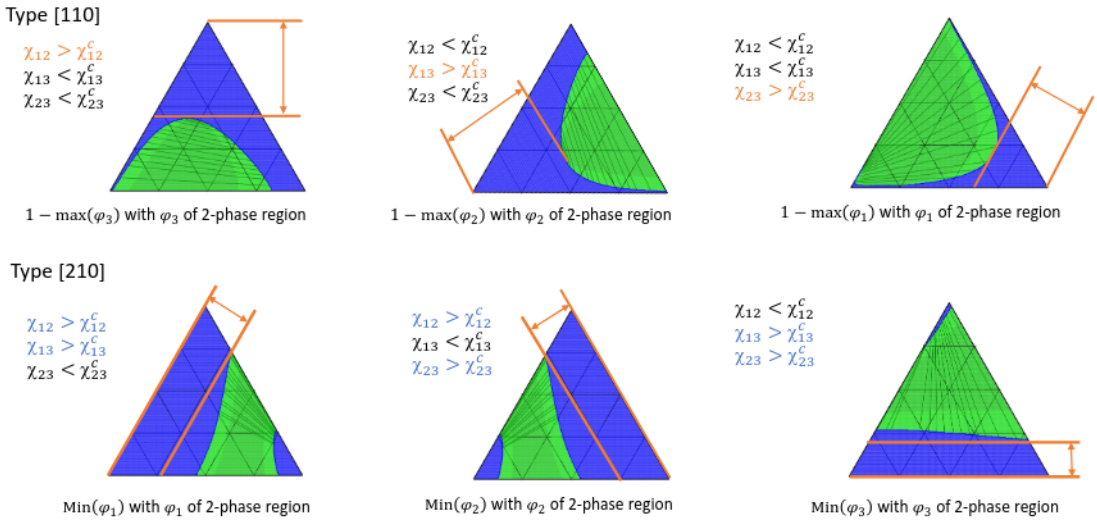

Figure 14: Characteristic quantities extracted from phase diagrams for type [110] (top) and [210] (bottom).

SI-5: Parameters used for each type of phase diagram identified

The following table gives the material parameters used to reproduce the different types of phase diagrams identified in the main text. The density is fixed to 1000 $kg\ m^{-3}$ for all the materials.

Table 2: Material parameters to illustrate the different types of phase diagrams identified

Phase diagram type	**Molar size**	**Interaction parameters**
[100]	$N_1 = 245, N_2 = 5, N_3 = 1$	$\chi_{12} = 0.0121, \chi_{13} = 0.0525, \chi_{23} = 0.0971$
$[110 - o]$	$N_1 = 5, N_2 = 1, N_3 = 1$	$\chi_{12} = 1.0472, \chi_{13} = 0.9949, \chi_{23} = 1.8699$
[110]	$N_1 = 5, N_2 = 1, N_3 = 1$	$\chi_{12} = 2.2837, \chi_{13} = 1.0472, \chi_{23} = 1.8699$
[131]	$N_1 = 5, N_2 = 1, N_3 = 1$	$\chi_{12} = 2.6565, \chi_{13} = 0.897, \chi_{23} = 1.8699$
[120]	$N_1 = 5, N_2 = 1, N_3 = 1$	$\chi_{12} = 1.1974, \chi_{13} = 0.8517, \chi_{23} = 2.1694$
[210]	$N_1 = 5, N_2 = 5, N_3 = 1$	$\chi_{12} = 0.42, \chi_{13} = 0.3172, \chi_{23} = 1.3784$
[141]	$N_1 = 5, N_2 = 5, N_3 = 1$	$\chi_{12} = 0.4339, \chi_{13} = 0.9949, \chi_{23} = 1.4782$
[231]	$N_1 = 5, N_2 = 1, N_3 = 1$	$\chi_{12} = 1.1974, \chi_{13} = 0.9791, \chi_{23} = 3.8145$
[162]	$N_1 = 1, N_2 = 1, N_3 = 245$	$\chi_{12} = 1.999, \chi_{13} = 1.0649, \chi_{23} = 1.0649$
[130]	$N_1 = 5, N_2 = 1, N_3 = 1$	$\chi_{12} = 1.3017, \chi_{13} = 1.2427, \chi_{23} = 2.2204$
[151]	$N_1 = 5, N_2 = 1, N_3 = 1$	$\chi_{12} = 1.3017, \chi_{13} = 1.3017, \chi_{23} = 2.2869$
[172]	$N_1 = 1, N_2 = 1, N_3 = 1$	$\chi_{12} = 2.6, \chi_{13} = 2.6, \chi_{23} = 2.6$
[193]	$N_1 = 1, N_2 = 1, N_3 = 1$	$\chi_{12} = 2.65, \chi_{13} = 2.65, \chi_{23} = 2.65$
[220]	$N_1 = 5, N_2 = 1, N_3 = 1$	$\chi_{12} = 1.1626, \chi_{13} = 2.2837, \chi_{23} = 2.6324$
[241]	$N_1 = 5, N_2 = 5, N_3 = 1$	$\chi_{12} = 0.4441, \chi_{13} = 1.0996, \chi_{23} = 1.6091$
[262]	$N_1 = 1, N_2 = 1, N_3 = 1$	$\chi_{12} = 2.7, \chi_{13} = 2.72, \chi_{23} = 2.63$
[283]	$N_1 = 1, N_2 = 1, N_3 = 1$	$\chi_{12} = 2.7, \chi_{13} = 2.7, \chi_{23} = 2.65$
[331]	$N_1 = 1, N_2 = 1, N_3 = 1$	$\chi_{12} = 2.1694, \chi_{13} = 2.3734, \chi_{23} = 3.8145$
[352]	$N_1 = 1, N_2 = 1, N_3 = 1$	$\chi_{12} = 2.63, \chi_{13} = 2.75, \chi_{23} = 2.8$
[373]	$N_1 = 1, N_2 = 1, N_3 = 1$	$\chi_{12} = 2.67, \chi_{13} = 2.7, \chi_{23} = 2.65$
[463]	$N_1 = 5, N_2 = 1, N_3 = 1$	$\chi_{12} = 1.6081, \chi_{13} = 1.6081, \chi_{23} = 2.2204$

SI-6: Parameters used for the modeling of experimental phase diagrams

For the different systems studied, the molar sizes $N_i = \frac{v_i}{v_0}$ are calculated using the species molar volumes $v_i = \frac{M_i}{\rho_i}$, where M_i and ρ_i are the species molar mass and density available from literature data, respectively. The values used for all studied material systems are summarized in Table 3. Note that the temperature dependence of the density is taken into account for the PS/NE/MCH and PS/EGDA/MCH mixtures.

Table 3: Material systems properties

Mixture	**Density** ($kg\ m^{-3}$)	**Molar mass** ($kg\ mol^{-1}$)	**Molar size**
n-hexane (1)	$\rho_1 = 613.4\ [22]$	$M_1 = 86.18 * 10^{-3}$	$N_1 = 1.24$
PMMA(2)	$\rho_2 = 1153\ [22]$	$M_2 = 50\ [22]$	$N_2 = 384$
MMA (3)	$\rho_3 = 886.8\ [22]$	$M_3 = 100.121 * 10^{-3}$	$N_3 = 1$
n-hexane(1)	$\rho_1 = 613.4\ [26]$	$M_1 = 86.18 * 10^{-3}$	$N_1 = 1.90$
acetone (2)	$\rho_2 = 784\ [26]$	$M_2 = 58.08 * 10^{-3}$	$N_2 = 1$
PMMA (3)	$\rho_3 = 1153\ [26]$	$M_3 = 159.97\ [26]$	$N_3 = 1873$
MCH (1)	$\rho_1 = 786.36 - 0.8479 * 10^{-1} * T - 3.75 * 10^{-4} * T^2\ [28]$	$M_1 = 98.186 * 10^{-3}$	$N_1 = 1$
NE (2)	$\rho_2 = 1073.06 - 1.1922 * 10^{-1} * T - 3.65 * 10^{-4} * T^2\ [28]$	$M_2 = 75.07 * 10^{-3}$	$N_2 = 1.09$
PS (3)	$\rho_3 = 1086.5 - 6.19 * 10^{-1} * T + 1.36 * 10^{-4} * T^2\ [28]$	$M_3 = 96.4\ [28]$	$N_3 = \frac{981.81 * \rho_1(T)}{\rho_3(T)}$
MCH (1)	$\rho_1 = 769.37\ [27]$	$M_1 = 98.186 * 10^{-3}$	$N_1 = 1$
EGDA (2)	$\rho_2 = 1106.3\ [27]$	$M_2 = 146.142 * 10^{-3}$	$N_2 = 1.04$
PS (3)	$\rho_3 = 1086.5 - 6.19 * 10^{-1} * T + 1.36 * 10^{-4} * T^2\ [27]$	$M_3 = 48\ [27]$	$N_3 = \frac{3.76 * 10^5}{\rho_3(T)}$

PMMA/MMA/n-hexane phase diagram

The interaction parameter values χ_{ij} measured by Jung and coworkers[22] are used for the phase diagram calculation (first row and last column of Figure 8). The critical interaction parameters χ_{ij}^c are calculated using equation 2. For this studied system, one interaction parameter is above the critical values (see Table 4).

Table 4: n-hexane (1), PMMA (2), MMA (3) interaction parameters

Interaction parameter	**Critical interaction parameter**
$\chi_{12} = 1.31\ [22]$	$\chi_{12}^c = 0.45$
$\chi_{13} = 1.49\ [22]$	$\chi_{13}^c = 1.8$
$\chi_{23} = 0.412\ [22]$	$\chi_{23}^c = 0.55$

PMMA/acetone/n-hexane phase diagram

The interaction parameters are determined experimentally with volume fraction dependency by Lai and coworkers[26] and are shown in the first column of Table 5. For the whole composition space, two interaction parameters are above the critical values (compare columns 1 and 3 of Table 5). Using this constraint, the PMMA/acetone/n-hexane phase diagram is calculated (second row and last column of Figure 8) using the interaction parameters values shown in the second column of Table 5.

Table 5: n-hexane (1), PMMA (2), MMA (3) interaction parameters

Interaction parameter from experiments	**Interaction parameter for modeling**	**Critical interaction parameter**
$\chi_{12}^{exp} = 1.574 + \frac{2.277}{1+3.026\varphi_2}$ [26]	$\chi_{12}^{mod} = 1.495$	$\chi_{12}^{c} = 1.49$
$\chi_{13}^{exp} = 2.07$ [26]	$\chi_{13}^{mod} = 0.58$	$\chi_{13}^{c} = 0.28$
$\chi_{23}^{exp} = 0.25 + 0.12\varphi_3$ [26]	$\chi_{23}^{mod} = 0.37$	$\chi_{23}^{c} = 0.52$

PS/MCH/EGDA phase diagram

At the measured phase diagrams temperatures (32.9°C, 33°C, 34°C, and 34.8 °C), the interaction parameters evaluated using Hildebrand solubilities are given in Table 6. The critical interaction parameters measured experimentally using Hildebrand solubilities and the binodal critical temperatures[27] are $\chi_{12}^{c,exp} = 1.66$, $\chi_{13}^{c,exp} = 0.54$, and $\chi_{23}^{c,exp} = 0.27$. Three interaction parameters are above the critical values for the four considered temperatures. The PS/MCH/EGDA phase diagrams are calculated (fourth row and last column of Figure 8) at different temperatures respecting this constraint but for the critical interaction parameters obtained from the molar sizes given in Table 3 ($\chi_{12}^{c} = 1.97$, $\chi_{13}^{c} = 0.55$, and $\chi_{23}^{c} = 0.54$). The interaction parameter values used for the calculation are given in Table 7.

Table 6: Measured interaction parameters from experiments for the MCH (1), EGDA (2), PS (3) mixture

Temperature / Interaction parameter	**32.9°C**	**33°C**	**34°C**	**34.8°C**
χ_{12}^{exp} [27]	1.6867	1.6861	1.6806	1.6763
χ_{13}^{exp} [27]	0.5460	0.5458	0.5441	0.5426
χ_{23}^{exp} [27]	0.3134	0.3133	0.3122	0.3114

Table 7: Interaction parameters used for modeling the MCH (1), EGDA (2), PS (3) phase diagrams

Temperature / Interaction parameter	**32.9°C**	**33°C**	**34°C**	**34.8°C**
χ_{12}^{mod}	2.15	2.15	2.0243	2.0129
χ_{13}^{mod}	0.567	0.562	0.563	0.56471
χ_{23}^{mod}	0.7	0.7	0.549	0.548

PS/MCH/NE phase diagram

Similar to PS/MCH/EGDA, the critical interaction parameters measured experimentally using Hildebrand solubilities and the binodal critical temperatures[28] are $\chi_{12}^{c,exp} = 3.08$, $\chi_{13}^{c,exp} = 0.51$, and $\chi_{23}^{c,exp} = 0.96$. At the measured phase diagrams temperatures (2.5°C, 3°C and 3.3°C), the interaction parameters using Hildebrand solubilities are available in Table 8. Three interaction parameters are above the critical values for the three considered temperatures. Here again, the phase diagrams are calculated (third row and last column of Figure 8) at different temperatures respecting this constraint, but for the critical interaction parameters obtained from the molar sizes given in Table 3 ($\chi_{12}^{c} = 1.92$, $\chi_{13}^{c} = 0.54$, and $\chi_{23}^{c} = 0.50$). The interaction parameter values used for the calculation are given in Table 9.

Table 8: Interaction parameters from experiments for the MCH (1), NE (2), PS (3) mixture

Temperature / Interaction parameter	**2.5°C**	**3°C**	**3.3°C**
χ_{12}^{exp} [28]	3.3144	3.3086	3.3051
χ_{13}^{exp} [28]	0.5923	0.5922	0.5916
χ_{23}^{exp} [28]	1.1032	1.1012	1.1001

Table 9: Interaction parameters used for modeling the MCH (1), NE (2), PS (3) phase diagrams

Temperature / Interaction parameter	**2.5°C**	**3°C**	**3.3°C**
χ_{12}^{mod}	2.2	2.2	2.2
χ_{13}^{mod}	1.2	1.2	1.2
χ_{23}^{mod}	0.65	0.65	0.59